Progress In Electromagnetics Research B, Vol. 66, 123–141, 2016

The Forward Transmission Matrix (FTM) Method for S-Parameter Analysis of Microwave Circuits and Their Metamaterial Counterparts

Omar F. Siddiqui[1, 2, *]

Abstract—In classical Electromagnetics textbooks, microwave circuits such as circulators, couplers, and filters are solved by non-systematic approaches such as even-odd mode analysis. Hence an electrical engineering student coming from the conventional circuit theory background encounters difficulties in understanding and solving microwave circuits. In this paper, we propose a modified node voltage analysis method in which the circuit branches are represented by their forward transmission matrices so that the electromagnetic wave propagation is taken care of. The Kirchhoff's current rule, tailored for high frequencies, is applied to formulate the simultaneous node voltage equations which are subsequently solved by matrix inversion. The proposed forward transmission matrix (FTM) method is applied to evaluate the S-parameters of some well-known microwave devices including the recently-developed metamaterial-based circuits. The FTM node analysis is a natural extension of the classical node analysis which is taught in the early stages of an Electrical Engineering program. Hence we anticipate that the proposed method will ease up the conceptual transition of electrical engineering students and academicians from the low-frequency alternating current circuits to high frequency RF and microwave circuits.

1. INTRODUCTION

The node voltage analysis is a widely used method to solve alternating or direct current (ac or dc) electrical circuits [1, 2]. However, it breaks down when tried to be used with circuits dimensionally comparable to the wavelength of the source voltage [3, 4]. Fig. 1 illustrates the difference of current flow between two nodes in a conventional ac circuit and a high frequency (microwave) circuit. In the conventional ac circuit (the long-wavelength regime), one global ground reference can be defined to which all the node voltages can be referred to (Fig. 1(a)). Hence the inter-nodal current can be simply calculated by dividing the difference of the adjacent node voltages by the total impedance seen by the current. In the microwave circuit (the short wave-length regime), one global ground cannot be defined because the fact that the electric field is non-conservative. In other words, there is a time lapse between the state of first node to affect the state of another spatially separated node, as predicted by the telegrapher's equations [3–6]. To account for the time lapse between the states of the nodes, a local ground node can be defined to each circuit node to which the node voltage can be referred [3]. Following this approach, the network characterization of port-based was performed and a locally-referenced $(M+1)\times(M+1)$ admittance matrix equation was generated for an M-port microwave circuit. The port voltages and currents could then be found by any numerical method [3]. Although quite suitable for commercial circuit analysis tools and harmonic balance simulators, the method does not

Received 21 January 2016, Accepted 13 March 2016, Scheduled 18 March 2016

* Corresponding author: Omar F. Siddiqui (omarsiddiqui2@gmail.com).

[1] Department of Electrical Engineering, College of Engineering, Taibah University, Madinah, Saudi Arabia. [2] Department of Electrical and Computer Engineering, University of Waterloo, Waterloo, ON N2L 3G1, Canada.

follow the systematic approach of the conventional nodal analysis procedure in which simultaneous nodal equations are deduced by the Kirchhoff's circuital laws. Therefore, it has not been adopted by popular textbooks to analyze the microwave devices such as directional couplers, power dividers, circulators and filters [5, 6]. The classical microwave textbooks usually resort to less methodical approaches such as the even-odd analysis [5] or the Π-T network representation for the S-parameter solution. Therefore, the engineering students transitioning from the classical to the high-frequency circuits are not able to connect the basic circuit courses with the advanced level electromagnetic and microwave courses.

In this paper, we aim to bridge this transition by providing the students an analysis method which is rooted in the basic electrical engineering methods of nodal analysis and Kirchhoff's circuit rules. The paper also serves as an introduction to the design and operation of the metamaterials-based devices [7–24] which will be analyzed using the proposed method along with their conventional equivalents. We develop a systematic nodal analysis approach based on the Kirchhoff's current rule which is tailored to the high frequency networks by $ABCD$ matrix representation of the circuit branches. Similar methodology has been earlier applied to analyze 2D periodic structures [22]. In the proposed technique, which will be further referred to as the FTM method, the circuit branches are represented by their forward transmission matrices, also known as the $ABCD$ matrices [5, 6]. Since the $ABCD$ matrix inherently takes into account the underlying electromagnetic wave propagation, the proposed method can be utilized for a very wide frequency spectrum. The paper is organized as follows. The modified Kirchhoff's current law is developed for the locally referenced nodes in Section 2. Section 3 serves two purposes. Firstly, a metamaterial unit cell is designed by applying the theory of periodic structures. Secondly, it introduces the FTM nodal method to analyze the metamaterial unit cell and operation of a metamaterial unit cell. The s-parameters are calculated by first inverting the **F**-matrix which is generated from the nodal equations. Section 4 presents the generalized rules to write **F**-matrix for an arbitrary microwave circuit. In Section 5, S-parameter calculations are performed using FTM analysis for several conventional microwave devices and their metamaterial counterparts. Finally, Section 6 is dedicated for the concluding remarks.

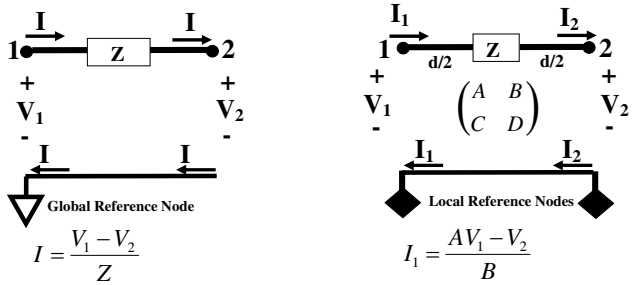

(a) Conventional ac circuit node (b) A High frequency (microwave) circuit node

Figure 1. The difference between the conventional node analysis and the high frequency node analysis.

2. THE KIRCHHOFF'S CURRENT LAW FOR THE NETWORKS REPRESENTED BY *ABCD* MATRICES

In Fig. 1(b), consider the spatial extension between node 1 and node 2 modeled as two transmission line segments with characteristic impedances of Z_0 and lengths of $d/2$ connected through a lumped impedance Z. The combined ABCD matrix can be written as follows:

$$\begin{pmatrix} A & B \\ C & D \end{pmatrix} = \begin{pmatrix} \cos\dfrac{\beta d}{2} & jZ_0 \sin\dfrac{\beta d}{2} \\ jY_0 \sin\dfrac{\beta d}{2} & \cos\dfrac{\beta d}{2} \end{pmatrix} \begin{pmatrix} 1 & Z \\ 0 & 1 \end{pmatrix} \begin{pmatrix} \cos\dfrac{\beta d}{2} & jZ_0 \sin\dfrac{\beta d}{2} \\ jY_0 \sin\dfrac{\beta d}{2} & \cos\dfrac{\beta d}{2} \end{pmatrix} \tag{1}$$

which after multiplication results in:

$$\begin{pmatrix} A & B \\ C & D \end{pmatrix} = \begin{pmatrix} \cos\beta d + j0.5Y_0 Z \sin\beta d & Z\cos^2\dfrac{\beta d}{2} + jZ_0 \sin\beta d \\ -jY_0^2 Z \sin\beta d + jY_0 \sin\beta d & \cos\beta d + j0.5Y_0 Z \sin\beta d \end{pmatrix} \tag{2}$$

where $\beta = 2\pi f/c$ is the phase constant and βd the phase incurred in the interconnecting transmission line segments between the two adjacent nodes. The voltages and currents at the nodes 1 and 2 can be written in terms of the combined $ABCD$ matrix in the following way:

$$\begin{pmatrix} V_2 \\ -I_2 \end{pmatrix} = \begin{pmatrix} A & B \\ C & D \end{pmatrix} \begin{pmatrix} V_1 \\ -I_1 \end{pmatrix} \tag{3}$$

Hence the current flowing out of node 1 towards node 2 can be written as follows:

$$I_1 = \frac{AV_1 - V_2}{B} \tag{4}$$

Note that in the long wavelength range (low frequencies) $\beta d \approx 0$ and A and B parameters in the matrix Equation (2) can be approximated to 1 and Z, respectively. The above nodal equation in this case reduces to:

$$I_1 = \frac{V_1 - V_2}{Z} \tag{5}$$

The outgoing current (4) obtained by the locally referenced $ABCD$ matrix equation very closely resembles to the familiar current Equation (5) obtained during the conventional ac nodal analysis.

3. THE METAMATERIAL UNIT CELL DESIGN AND ITS NODAL ANALYSIS

Metamaterials have stirred up exciting new dimensions in the fields of Electromagnetics and Physics in the past decade [7–24]. Here we focus on metamaterial transmission lines (TL) also known as left-handed transmission lines [9, 10, 13–24]. On account of their unique dispersion characteristics, metamaterial-TLs have been employed in building compact microwave devices, filters, compact phase shifters, and miniaturized [14–20] antennas. In the modern communication system design, these lines have attracted widespread interest on account of their tuneable frequency response which can be arbitrarily designed to occupy certain bands that are not harmonically related [14, 15]. They can also be designed to reject harmonically occurring frequency bands that cause unnecessary interference and power spill-over resulting in power losses [20]. The cleared bands can then be used for other applications. A metamaterial-TL can be designed by periodically repeating either of the two unit cells depicted in Fig. 2. A unit cell of Fig. 2(a) is composed of a host line segment of length d and impedance Z_U loaded in series with capacitor and in shunt with an inductor L_{sh}. An extra capacitive shunt is added in Fig. 2(b) to achieve design compactness and better bandwidth control of the rejection band [20]. The metamaterial design presented here will be subsequently used in Section 4 to analyze microwave devices.

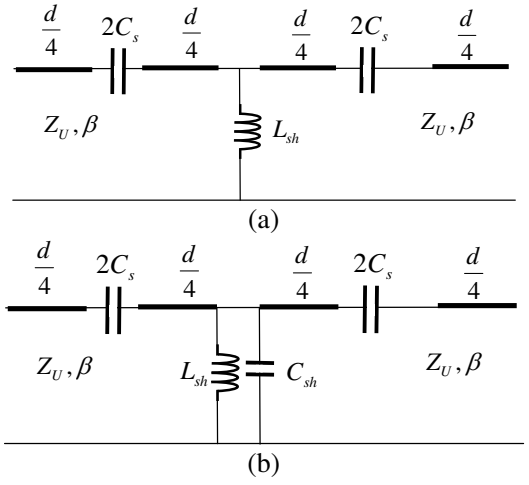

Figure 2. Unit cell of a capacitor-loaded TL-metamaterial The extra shunt capacitor provides controllable bandpass characteristics.

3.1. Metamaterial Unit Cell Design

Consider a metamaterial-TL design having a Bloch impedance of 50 Ω and 22.5° Bloch phase shift (shift per unit cell) and a rejection band between 1.2 GHz and 2.5 GHz. The component values for Fig. 2(a) unit cell can be calculated by following the design approach outlined in Appendix A [20]. To verify the correctness of the design procedure, the Brillouin diagram is depicted in Fig. 3 which is drawn for the design parameters provided in the inset. The design frequency of 0.9 GHz lies within the lowest fundamental band (i.e., 1.2 GHz). Note that the electromagnetic wave in this band takes place as a backward-wave mode which is identified by the negative slope of the Brillouin diagram and is the hallmark of left-handed metamaterial-TLs [7, 8, 16]. The design criteria of 0.125π phase shift at 0.9 GHz and the stop band between 1.2 and 2.5 GHz are indeed satisfied. In the second passband, which is the region above 2.5 GHz, the usual forward-wave propagation takes place.

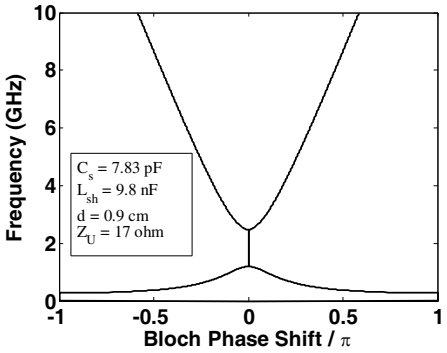

Figure 3. The Brillouin Diagram showing the relation between frequency and unit cell phase shift (Bloch phase shift) of a metamaterial line.

3.2. The FTM Nodal Analysis of the Metamaterial Unit Cell

Consider a 3-node metamaterial unit cell connected to a sinusoidal source and a load depicted in Fig. 4 and its low-frequency equivalent in Fig. 5. Referring each node voltage to its local reference node, the application of the KCL results in the following three nodal equations:

$$\frac{A_{Cx1}V_1 - V_2}{B_{Cx1}} + \frac{V_1 - V_S}{R_S} = 0 \tag{6}$$

$$\frac{A_{Cx1}V_2 - V_1}{B_{Cx1}} + \frac{A_{Ly1}V_2}{B_{Ly1}} + \frac{A_{Cx2}V_2 - V_3}{B_{Cx2}} = 0 \tag{7}$$

$$\frac{A_{Ry1}V_3}{B_{Ry1}} + \frac{A_{Cx2}V_3 - V_2}{B_{Cx2}} = 0 \tag{8}$$

The forward transmission matrix elements used in Equations (6)–(8) can be obtained by multiplying the respective lumped element matrices with the transmission line matrix, as given in Fig. 4(a). The above system of linear equations can be rearranged to give the solution of the unknown voltages:

$$\mathbf{V} = \mathbf{F}^{-1}\mathbf{V}_S \tag{9}$$

where **F**-matrix consists of the A and B elements of the forward transmission matrix constituting the branches of the microwave circuit, given by:

$$\bar{F} = \begin{pmatrix} \dfrac{A_{Cx1}}{B_{Cx1}} + \dfrac{1}{R_S} & -\dfrac{1}{B_{Cx1}} & 0 \\ -\dfrac{1}{B_{Cx1}} & \dfrac{A_{Cx1}}{B_{Cx1}} + \dfrac{A_{Ly1}}{B_{Ly1}} + \dfrac{A_{Cx2}}{B_{Cx2}} & -\dfrac{1}{B_{Cx2}} \\ 0 & -\dfrac{1}{B_{Cx2}} & \dfrac{A_{Cx2}}{B_{Cx2}} + \dfrac{A_{Ry1}}{B_{Ry1}} \end{pmatrix} \tag{10}$$

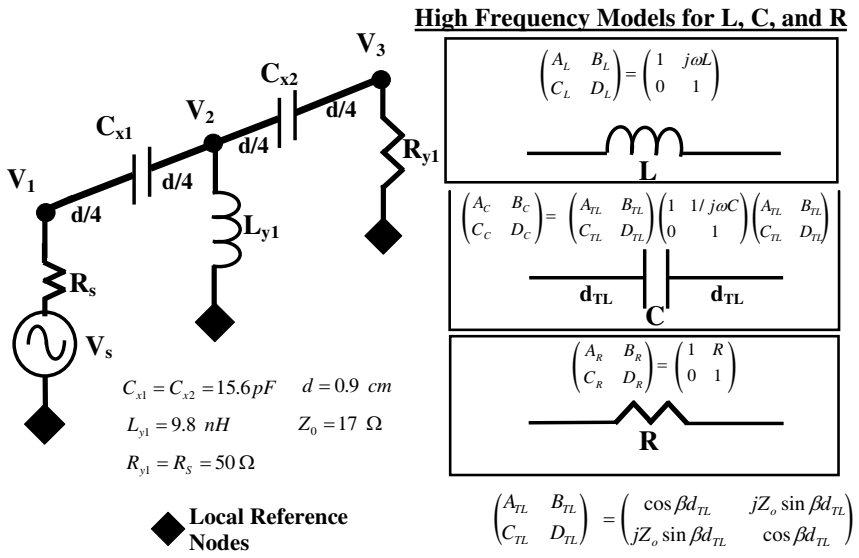

Figure 4. A left-handed transmission line (metamaterial) unit cell as seen at microwave frequencies (Forward Transmission Matrix model).

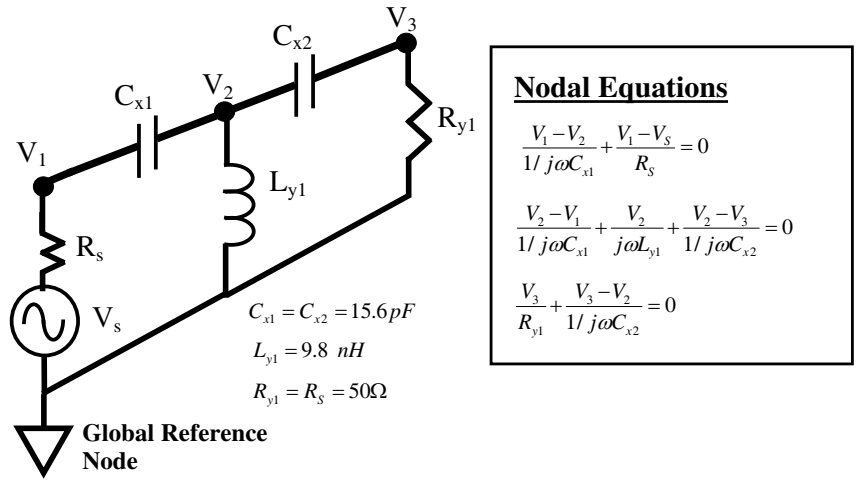

Figure 5. Low frequency (long-wavelength) view of an the metamaterial unit cell (conventional model).

V and $\mathbf{V_s}$ are the node voltage and source voltage arrays given by:

$$\bar{V} = (V_1 \quad V_2 \quad V_3)^T \quad \text{and} \quad \bar{V}_S = (V_s/R_s \quad 0 \quad 0)^T \tag{11}$$

For comparison, see the associated nodal equations for the low-frequency model shown in the inset of Fig. 5. These equations can also be obtained from Equations (6)–(8) by assuming the long-wavelength limit ($\beta d \approx 0$). The **F**-matrix Equation (9) along with low-frequency nodal equations are solved numerically for a frequency range 0 to 10 GHz, and the results are depicted in Fig. 6. The microwave circuit is also simulated using the commercially available high frequency circuit simulator Agilent-ADS, and the results are superimposed in Fig. 6 plots. As shown, the numerically generated results using the FTM model are in full agreement with the ones generated by ADS. Towards the dc frequency range where the transmission line segments are much shorter than the wavelength, the lumped component behavior is dominant, and the conventional ac model and the FTM model give similar results. At 900 MHz frequency, the matching conditions are met as the designed Bloch impedance of the metamaterial-TL becomes equal to the load impedance. Consequently, the load voltage V_3 predicted by the microwave model becomes maximum. With the increase of frequency, there is a decrease in the

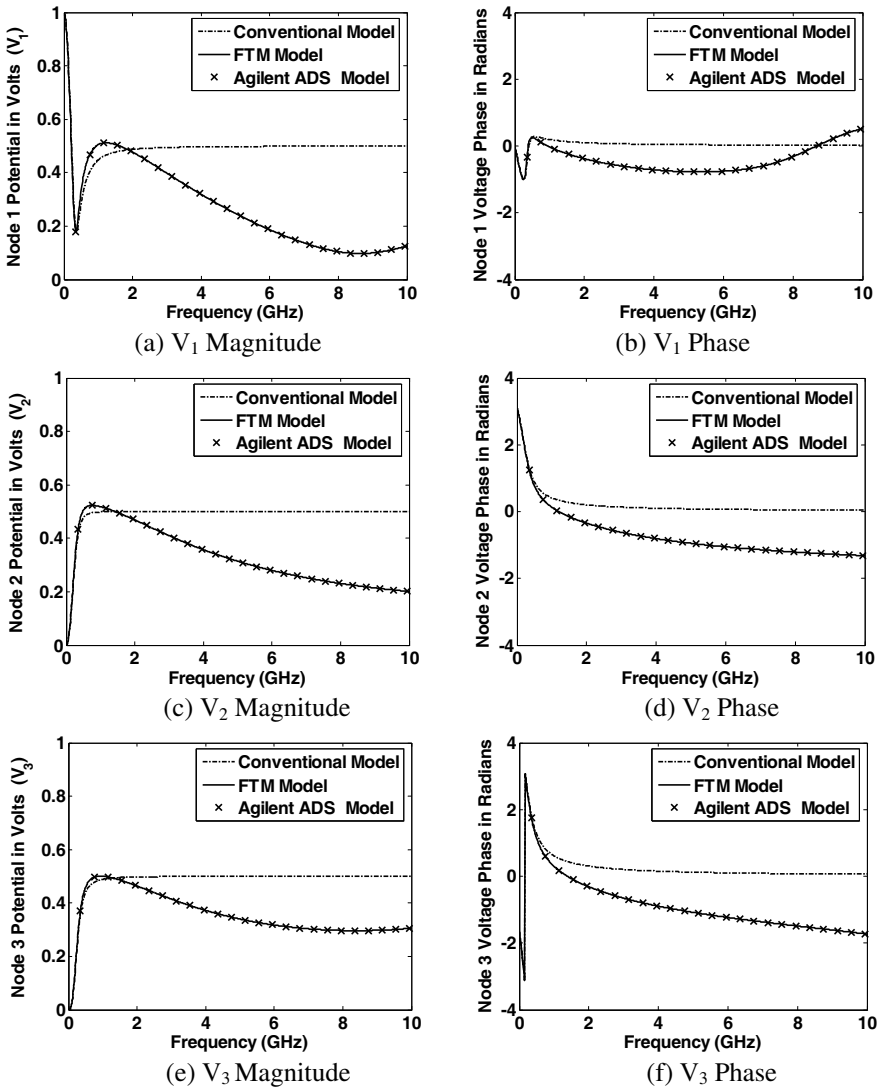

(a) V_1 Magnitude (b) V_1 Phase

(c) V_2 Magnitude (d) V_2 Phase

(e) V_3 Magnitude (f) V_3 Phase

Figure 6. The low and high frequency node voltage solution for the metamaterial unit cell given in Figs. 4 and 5.

capacitive reactance ($1/j\omega C$) and an increase in the inductive reactance ($j\omega L$). Beyond approximately 2 GHz, the shunt inductor and series capacitor can be respectively approximated as an open and a short circuits, and the output voltage V_3 across the resistor R_{y1} in the conventional model assumes a steady 0.5 V and an approximate phase angle of $\angle 0°$. At these frequencies, the FTM model predicts a different behavior of the node voltages due to the distributed transmission line impedances seen by the propagating wave. These impedance mismatches result in the magnitude fluctuations and phase changes that are not captured by the conventional node analysis. In particular, consider the difference between the phase propagation of the fundamental backward-wave mode and the second-harmonic forward-wave mode propagation observed in the Brillouin dispersion diagram of Fig. 3. The difference can be well demonstrated by knowing the phase difference between nodes 1 and 3 obtained from the FTM model in the two frequency bands. At 900 MHz, which lies in the fundamental band (see Fig. 3), the phase is accumulated at node 3 as the wave propagates from input towards the load. Hence the node voltage V_3 ($0.51\angle 23°$) leads the node voltage V_1 ($0.49\ \angle 1.4°$) by 21.6° indicating a backward-wave propagation. On the other hand, at 6 GHz, the transmission phase depreciates with wave propagation. Therefore, the voltage at node 3 ($0.28\angle -70.5°$) lags node 1 voltage ($0.187\angle -43°$ by 27.5°) which indicates a forward-wave propagation.

4. THE F-MATRIX GENERATION RULES

The **F**-matrix consists of coefficients of the node voltage equations comprising the elements of $ABCD$ matrices representing the branches of a high frequency electrical network. For example, the **F**-matrix of the set of Equations (6)–(8) for the metamaterial unit cell is given by Equation (10). For an N-node network, a $N \times N$ matrix is needed to be solved. The general configuration of the **F**-Matrix is given below.

$$\bar{F} = \begin{pmatrix} F_{11} & F_{12} & F_{13} & \bullet & \bullet & F_{1N} \\ F_{21} & F_{22} & F_{23} & \bullet & \bullet & F_{2N} \\ F_{31} & F_{32} & F_{33} & \bullet & \bullet & F_{3N} \\ \bullet & \bullet & \bullet & \bullet & \bullet & \bullet \\ \bullet & \bullet & \bullet & \bullet & \bullet & \bullet \\ F_{N1} & F_{N2} & F_{N3} & \bullet & \bullet & F_{NN} \end{pmatrix} \tag{12}$$

Looking at the high frequency circuit of Fig. 4 and its **F**-matrix in Equation (10), the correspondence between the voltage nodes and the elements of the matrix can be readily established. If $m = n$, F_{mn} are given by:

$$F_{mn} = \sum_{n=1}^{N} X_{mn} \frac{A_{mn}}{B_{mn}}, \quad m = 1, 2, ...N \tag{13}$$

For matrix entries $m \neq n$,

$$F_{mn} = -X_{mn} \frac{1}{B_{mn}}, \quad m = 1, 2, \ldots N \tag{14}$$

where A_{mn} and B_{mn} are the forward transmission elements of the branch connecting the nodes m and n, as shown in Fig. 7. X_{mn} is the connection indicator which, if $X_{mn} = 1$, indicates the presence of connection between nodes m and n and indicates a lack thereof when $X_{mn} = 0$.

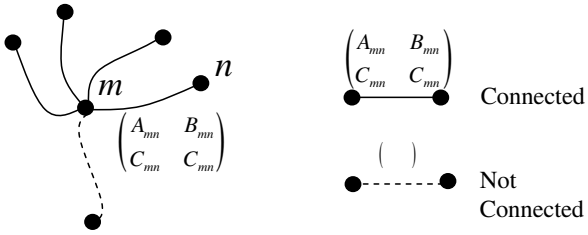

Figure 7. The generation of **F**-matrix by examining the connection between the nodes and its forward transmission matrix.

5. MICROWAVE NODAL ANALYSIS OF MICROWAVE DEVICES

5.1. The Quadrature Hybrid

The quadrature hybrid is a directional coupler extensively used in microwave engineering for power division, impedance matching, and isolation purposes. Consider the conventional quadrature-hybrid directional coupler depicted in Fig. 8(a) and its metamaterial equivalent in Fig. 8(b). The coupler consists of four transmission-line sections extending a quarter-wave length transmission line sections. The input power is equally divided between through port 2 and coupled port 3, and the two ports are 90° out of phase with respect to each other. In this section, the S-parameters of the conventional and metamaterial couplers are compared by the FTM method formulated in the previous sections.

5.1.1. The Quadrature Hybrid F-matrix

Looking at Fig. 8 and short circuiting the voltage source, it can be observed that all the nodes are connected to one x-, one y-directed branch and a resistor Z_o:

$$F_{11} = F_{22} = F_{33} = F_{44} = \frac{A_x}{B_x} + \frac{A_y}{B_y} + \frac{A_Z}{B_Z} \tag{15}$$

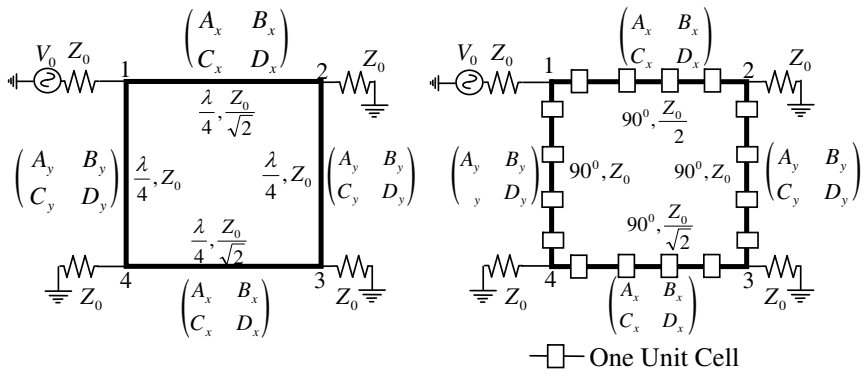

(a) Conventional Quadrature Hybrid (b) Metamaterial Quadrature Hybrid

Figure 8. (a) The conventional quadrature hybrid directional coupler. (b) The metamaterial quadrature hybrid where the transmission line segments are replaced by four unit cells of left-handed transmission line.

where $A_Z/B_Z = 1/Z_o$ represents the port impedance Z_o. Furthermore, nodes 1 with 2 and nodes 3 with 4 are connected by x-directed segments which can be translated to the following matrix:

$$F_{12} = F_{21} = F_{34} = F_{43} = -\frac{1}{B_x} \tag{16}$$

$$F_{23} = F_{32} = F_{14} = F_{41} = -\frac{1}{B_y} \tag{17}$$

Since no connection exists between nodes 1-3 and 2-4, the corresponding matrix entries are zero:

$$F_{13} = F_{31} = F_{24} = F_{42} = 0 \tag{18}$$

Therefore, the **F**-matrix can be written by combining Equations (15)–(18), as follows:

$$\bar{F} = \begin{pmatrix} \frac{A_x}{B_x} + \frac{A_y}{B_y} + \frac{A_Z}{B_Z} & -\frac{1}{B_x} & 0 & -\frac{1}{B_y} \\ -\frac{1}{B_x} & \frac{A_x}{B_x} + \frac{A_y}{B_y} + \frac{A_Z}{B_Z} & -\frac{1}{B_y} & 0 \\ 0 & -\frac{1}{B_y} & \frac{A_x}{B_x} + \frac{A_y}{B_y} + \frac{A_Z}{B_Z} & -\frac{1}{B_x} \\ -\frac{1}{B_y} & 0 & -\frac{1}{B_x} & \frac{A_x}{B_x} + \frac{A_y}{B_y} + \frac{A_Z}{B_Z} \end{pmatrix} \tag{19}$$

where $A_Z/B_Z = 1/Z_o$ represents the port impedance Z_o. The node voltages are given by applying Equation (9) where $\boldsymbol{V}$ and $\boldsymbol{V_s}$ assuming a source voltage of 1V are given by:

$$\bar{V} = (V_1 \quad V_2 \quad V_3 \quad V_4)^T \quad \text{and} \quad \bar{V}_S = (1/Z_0 \quad 0 \quad 0 \quad 0)^T \tag{20}$$

The 4×4 **F**-matrix can be obtained from the set of simultaneous Equations (12)–(15):

5.1.2. The S-Parameter Solution of a Conventional Quadrature Hybrid at the Design Frequency of 900 MHz

The forward transmission line matrices for x- and y-directed transmission line segments for the conventional hybrid are given by:

$$\begin{pmatrix} A_k & B_k \\ C_k & D_k \end{pmatrix} = \begin{pmatrix} \cos\beta L_k & jZ_{0n}\sin\beta L_k \\ jY_{0k}\sin\beta L_k & \cos\beta L_k \end{pmatrix} \tag{21}$$

where $k = x$ or y and L_k is the length of the transmission line segments between the nodes. Assuming system impedance $Z_0 = 50\,\Omega$, section impedances are given by $Z_{0x} = 50\,\Omega$ and $Z_{0y} = 35.35\,\Omega$. At the

design frequency of 0.90 GHz, length L_k becomes equal to $\lambda/4$ so that the phase shift βL_k attains a value of $\pi/2$, and the elements of the above $ABCD$ matrix are simplified to $A_k = D_k = 0$, $B_k = jZ_{ok}$ and $C_k = jY_{ok}$. The **F**-matrix and its inverse are then given by:

$$\bar{F} = \frac{1}{Z_0}\begin{pmatrix} 1 & j\sqrt{2} & 0 & j \\ j\sqrt{2} & 1 & j & 0 \\ 0 & j & 1 & j\sqrt{2} \\ j & 0 & j\sqrt{2} & 1 \end{pmatrix}, \quad \bar{F}^{-1} = -\frac{Z_0}{2\sqrt{2}}\begin{pmatrix} \sqrt{2} & j & 1 & 0 \\ j & \sqrt{2} & 0 & 1 \\ 1 & 0 & \sqrt{2} & j \\ 0 & 1 & j & \sqrt{2} \end{pmatrix} \tag{22}$$

The node voltages are found by multiplying the $\mathbf{F}^{-1}$ by the source array in Equation (20)

$$\begin{bmatrix} V_1 \\ V_2 \\ V_3 \\ V_4 \end{bmatrix} = -\frac{Z_0}{2\sqrt{2}}\begin{pmatrix} -\sqrt{2} & j & 1 & 0 \\ j & -\sqrt{2} & 0 & 1 \\ 1 & 0 & -\sqrt{2} & j \\ 0 & 1 & j & -\sqrt{2} \end{pmatrix}\begin{bmatrix} 1/Z_0 \\ 0 \\ 0 \\ 0 \end{bmatrix} = \begin{bmatrix} 1/2 \\ -j/2\sqrt{2} \\ -1/2\sqrt{2} \\ 0 \end{bmatrix} \tag{23}$$

The S-parameters can be extracted by the following transformation:

$$\begin{bmatrix} S_{11} \\ S_{21} \\ S_{31} \\ S_{41} \end{bmatrix} = \begin{bmatrix} 2V_1 - 1 \\ 2V_2 \\ 2V_3 \\ 2V_4 \end{bmatrix} = \begin{bmatrix} 0 \\ -j/\sqrt{2} \\ -1/\sqrt{2} \\ 0 \end{bmatrix} \tag{24}$$

The device is reciprocal and symmetric, hence $S_{nm} = S_{mn}$ and the 4×4 scattering matrix can be written as follows:

$$\bar{S} = -\frac{1}{\sqrt{2}}\begin{pmatrix} 0 & j & 1 & 0 \\ j & 0 & 0 & 1 \\ 1 & 0 & 0 & j \\ 0 & 1 & j & 0 \end{pmatrix} \tag{25}$$

Eq. (25) is the common device representation followed by the microwave textbooks such as [5]. It shows good matching ($S_{11} = 0$) and isolation ($S_{41} = 0$) at the design frequency of 900 MHz. The power entering node 1 is equally divided between node 2 (the through port) and node 3 (the coupled port) with a 90° phase shift as indicated by S_{21} and S_{31} values.

5.1.3. The Frequency-Domain S-Parameter Plots

To observe the device behavior at other frequencies, the S-parameters are plotted as functions of frequency by solving the original **F**-matrix given in Eqs. (19) and (9). The results are depicted in Fig. 9. At the design frequency, the equal power division and good isolation and reflection properties can

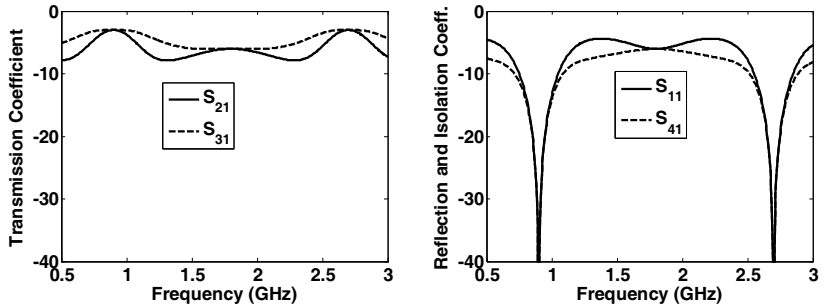

(a) Transmission Coefficient (b) Reflection and Isolation Coefficients

Figure 9. The simulation results for the conventional quadrature hybrid of Fig. 5(a). (a) The transmission coefficient of the through (S_{21}) and coupled (S_{31}) ports show equal power division at the fundamental frequency 0.75 GHz and the first harmonic 2.7 GHz. (b) The reflection coefficient (S_{11}) and the isolation (S_{41}) show good isolation and matching.

be seen. Since the transmission-line phase is a periodically repeatable phenomenon, the transmission characteristics of the coupler are also repeated at three times of the fundamental frequency, i.e., at 2.7 GHz the lengths of the transmission lines become $3\lambda/2$.

5.1.4. The S-Parameter Analysis of a Metamaterial Quadrature Hybrid

To suppress the higher order harmonics, the quarter-wavelength lines of the conventional quadrature hybrid are replaced by the metamaterial-TL segments designed to exhibit Bloch impedances of 50 and 35.35 Ω with shifts of 90°, as shown in Fig. 8(b). Assuming Bloch phase shift of 22.5° per unit cell and a stop band between 1.2 and 3 GHz, the parameters of Fig. 2(b) metamaterial unit cell are calculated by the design procedure illustrated in Appendix A and summarized in Table 1. The forward transmission matrix for the K-cell metamaterial-TL segment between the two coupler nodes can be obtained by first combining the forward matrices of the TL segments and lumped components of Fig. 2(b) unit call, and then repeating the combined matrix N times i.e.:

$$\begin{pmatrix} A_k & B_k \\ C_k & D_k \end{pmatrix} = \left([TL]_k\,[Z_S]\,[TL]_k\,[Y_{Sh}]\,[TL]_k\,[Z_S]\,[TL]_k\right)^K \tag{26}$$

where $k = x$ or y, K (here $K = 4$ is assumed), and the matrices are given by:

$$[TL]_k = \begin{pmatrix} \cos\dfrac{\beta d_k}{4} & jZ_{Uk}\sin\dfrac{\beta d_k}{4} \\ jY_{Uk}\sin\dfrac{\beta d_k}{4} & \cos\dfrac{\beta d_k}{4} \end{pmatrix} \tag{27}$$

$$[Z_{sh}] = \begin{pmatrix} 1 & Z_s \\ 0 & 1 \end{pmatrix}, \quad [Y_{sh}] = \begin{pmatrix} 1 & 0 \\ Y_{sh} & 1 \end{pmatrix} \tag{28}$$

where $Z_s = j\omega C_s$ and $Y_{sh} = j\omega C_{sh} + 1/j\omega L_{sh}$.

Table 1. The unit cell design of the metamaterial coupler.

n	$\mathbf{Z_{Bk}}$ **(0.9 GHz)**	$\theta_{\mathbf{Bk}}$ **(0.9 GHz)**	$\mathbf{Z_{Un}}$	$\mathbf{d_n}$	$\mathbf{C_s}$	$\mathbf{C_{sh}}$	$\mathbf{L_{sh}}$
x	50 Ω	$\pi/8$	20.9 Ω	0.49 cm	8.2 pF	1 pF	9.8 nH
y	35.35 Ω	$\pi/8$	21.5 Ω	0.34 cm	12.5 pF	2 pF	7 nH

At the design frequency of 900 MHz, the F matrix and its inverse attain the following form:

$$\bar{F} = \frac{1}{Z_0}\begin{pmatrix} 1 & -j\sqrt{2} & 0 & -j \\ -j\sqrt{2} & 1 & -j & 0 \\ 0 & -j & 1 & -j\sqrt{2} \\ -j & 0 & -j\sqrt{2} & 1 \end{pmatrix}, \quad \bar{F}^{-1} = \frac{Z_0}{2\sqrt{2}}\begin{pmatrix} \sqrt{2} & j & -1 & 0 \\ j & \sqrt{2} & 0 & -1 \\ -1 & 0 & \sqrt{2} & j \\ 0 & -1 & j & \sqrt{2} \end{pmatrix} \tag{29}$$

and the node voltages can be written as:

$$\begin{bmatrix} V_1 \\ V_2 \\ V_3 \\ V_4 \end{bmatrix} = \frac{Z_0}{2\sqrt{2}}\begin{pmatrix} \sqrt{2} & j & -1 & 0 \\ j & \sqrt{2} & 0 & -1 \\ -1 & 0 & \sqrt{2} & j \\ 0 & -1 & j & \sqrt{2} \end{pmatrix}\begin{bmatrix} 1/Z_0 \\ 0 \\ 0 \\ 0 \end{bmatrix} = \begin{bmatrix} 1/2 \\ j/2\sqrt{2} \\ -1/2\sqrt{2} \\ 0 \end{bmatrix} \tag{30}$$

which can be converted to the S-matrix by applying the transformation of Eq. (24) and using symmetry and reciprocity arguments:

$$\bar{S} = -\frac{1}{\sqrt{2}}\begin{pmatrix} 0 & -j & 1 & 0 \\ 1 & 0 & 0 & 1 \\ -j & 0 & 0 & -j \\ 0 & 1 & -j & 0 \end{pmatrix} \tag{31}$$

The transmission, reflection, and isolation parameters can also be calculated at other frequencies by applying the full solution using Eqs. (9), (19) and (20). As depicted in Fig. 10, the coupler demonstrates the equal power division at the designed frequency of 0.9 GHz. Comparing Figs. 9 and 10, it can be observed that the 2.7 GHz harmonic mode is well suppressed for the metamaterial coupler. The difference between the transmission power levels at the third harmonic frequency is more than 20 dB. As shown in Fig. 10(b), the S_{11} dip of -40 dB at the designed frequency shows good matching at the input port. Moreover, excellent isolation of more than 20 dB is obtained on port 4 of the coupler.

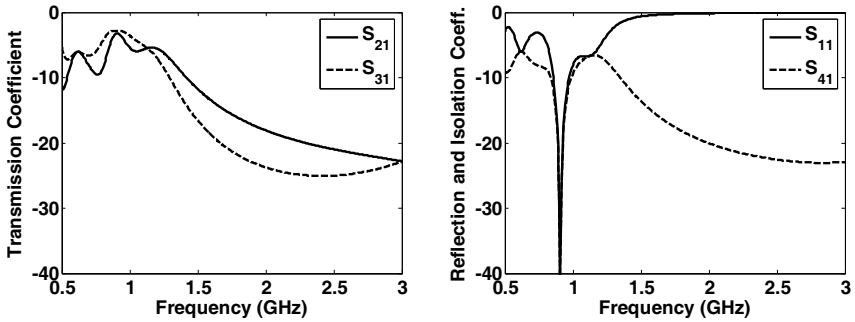

Figure 10. The simulation results for the metamaterial quadrature hybrid of Fig. 8(b). (a) The transmission coefficient of the through (S_{21}) and coupled (S_{31}) ports show equal power division at the fundamental frequency 0.9 GHz and harmonic suppression of 2.7 GHz mode. The Reflection coefficient (S_{11}) and the isolation (S_{41}) show good isolation and matching at the design frequency.

5.2. The 180° Ring Hybrid Coupler

A schematic diagram of a four-port ring hybrid and its metamaterial counterpart are given in Fig. 11. The ring hybrid is a powerful microwave device and can be used in several applications including power division, multiplexers, and demultiplexers [5, 6, 23]. An input power applied at port 1 is divided equally between ports 2 and 3 having a zero phase difference and an isolated port 4. The power applied at port 4 results in a power split at ports 2 and 3 with a 180° phase difference and an isolated port 1. If simultaneous signals are applied at ports 2 and 3, they are added at port 1 and subtracted at port 4.

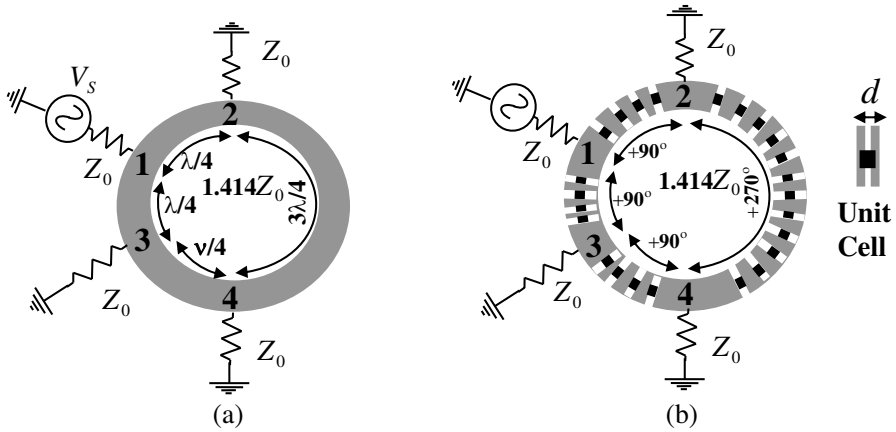

Figure 11. (a) The conventional 180° hybrid and (b) its metamaterial counterpart.

5.2.1. The F-Matrix and S-Parameter Solution at Design Frequency

The **F**-matrix can be generated by applying the generalized rules outlined in Section 4. Assuming that the short segments ($\lambda/4$) in Fig. 11 are represented by $ABCD$ matrix elements (A_1, B_1) and the long

segment ($3\lambda/4$) by (A_2, B_2), the **F**-matrix can be written as:

$$\bar{F} = \begin{pmatrix} 2\frac{A_1}{B_1} + \frac{A_Z}{B_Z} & -\frac{1}{B_1} & -\frac{1}{B_1} & 0 \\ -\frac{1}{B_1} & \frac{A_1}{B_1} + \frac{A_2}{B_2} + \frac{A_Z}{B_Z} & 0 & -\frac{1}{B_2} \\ -\frac{1}{B_1} & 0 & 2\frac{A_1}{B_1} + \frac{A_Z}{B_Z} & -\frac{1}{B_1} \\ 0 & -\frac{1}{B_2} & -\frac{1}{B_1} & \frac{A_1}{B_1} + \frac{A_2}{B_2} + \frac{A_Z}{B_Z} \end{pmatrix} \tag{32}$$

where $k = 1$ and 2 for the respective shorter and longer transmission lines. The $ABCD$ matrix elements A_k and B_k are given by $jZ_{ok}\cos\beta L_k$ and $jY_{ok}\sin\beta L_k$, respectively. Elements A_Z and B_Z are given by 1 and $Z_{o,}$, respectively. For the conventional ring hybrid, the characteristics impedances of the two types of transmission line segments are given by $Z_{o1} = Z_{o2} = 1.414Z_o$. For the metamaterial ring hybrid, the 90° and 270° segments are composed of four and twelve unit cells, respectively, with a Bloch shift of 22.5° per cell and the lumped components given in Table 2. At the design frequency of 900 MHz, the **F**-matrix and its inverse are simplified to:

$$\bar{F} = \frac{1}{Z_0}\begin{pmatrix} 1 & \pm\frac{j}{\sqrt{2}} & \pm\frac{j}{\sqrt{2}} & 0 \\ \pm\frac{j}{\sqrt{2}} & 1 & 0 & \mp\frac{j}{\sqrt{2}} \\ \pm\frac{j}{\sqrt{2}} & 0 & 1 & \pm\frac{j}{\sqrt{2}} \\ 0 & \mp\frac{j}{\sqrt{2}} & \pm\frac{j}{\sqrt{2}} & 1 \end{pmatrix}, \quad \bar{F}^{-1} = \frac{Z_0}{2\sqrt{2}}\begin{pmatrix} \sqrt{2} & \mp j & \mp j & 0 \\ \mp j & \sqrt{2} & 0 & \pm j \\ \mp j & 0 & \sqrt{2} & \mp j \\ 0 & \pm j & \mp j & \sqrt{2} \end{pmatrix} \tag{33}$$

where the *upper* sign indicates the conventional hybrid solution, and the *lower* sign denotes the metamaterial solution. Assuming the input at port 1, the port voltages for both the hybrids can be obtained as follows:

$$\begin{bmatrix} V_1 \\ V_2 \\ V_3 \\ V_4 \end{bmatrix} = \frac{Z_0}{2\sqrt{2}}\begin{pmatrix} \sqrt{2} & \mp j & \mp j & 0 \\ \mp j & \sqrt{2} & 0 & \pm j \\ \mp j & 0 & \sqrt{2} & \mp j \\ 0 & \pm j & \mp j & \sqrt{2} \end{pmatrix}\begin{bmatrix} 1/Z_0 \\ 0 \\ 0 \\ 0 \end{bmatrix} = \begin{bmatrix} 1/2 \\ \mp j/2\sqrt{2} \\ \mp j/2\sqrt{2} \\ 0 \end{bmatrix} \tag{34}$$

The S-parameters can be obtained by using the voltage to S-parameter transformation in Eq. (24),

$$\begin{bmatrix} S_{14} \\ S_{24} \\ S_{34} \\ S_{44} \end{bmatrix} = \begin{bmatrix} 2V_1 - 1 \\ 2V_2 \\ 2V_3 \\ 2V_4 \end{bmatrix} = \begin{bmatrix} 0 \\ \mp j/\sqrt{2} \\ \mp j/\sqrt{2} \\ 0 \end{bmatrix} \tag{35}$$

If the input is applied at port 4, the resulting voltages can be found by:

$$\begin{bmatrix} V_1 \\ V_2 \\ V_3 \\ V_4 \end{bmatrix} = \begin{bmatrix} S_{14}/2 \\ S_{24}/2 \\ S_{34}/2 \\ S_{44}/2 + 1/2 \end{bmatrix} = \frac{Z_0}{2\sqrt{2}}\begin{pmatrix} \sqrt{2} & \mp j & \mp j & 0 \\ \mp j & \sqrt{2} & 0 & \pm j \\ \mp j & 0 & \sqrt{2} & \mp j \\ 0 & \pm j & \mp j & \sqrt{2} \end{pmatrix}\begin{bmatrix} 0 \\ 0 \\ 0 \\ 1/Z_0 \end{bmatrix} = \begin{bmatrix} 0 \\ \pm j/2\sqrt{2} \\ \mp j/2\sqrt{2} \\ 1/2 \end{bmatrix} \tag{36}$$

The combined S-matrix can therefore be written as:

$$\bar{S} = \mp\frac{j}{\sqrt{2}}\begin{pmatrix} 0 & 1 & 1 & 0 \\ 1 & 0 & 0 & -1 \\ 1 & 0 & 0 & 1 \\ 0 & -1 & 1 & 0 \end{pmatrix} \tag{37}$$

Table 2. The unit cell design of the metamaterial ring hybrid.

n	Z_{Bk} (0.9 GHz)	θ_{Bk} (0.9 GHz)	Z_{Un}	d_n	C_s	C_{sh}	L_{sh}
1, 2	70.7 Ω	$\pi/8$	41.7 Ω	0.35 cm	5.8 pF	1 pF	13.7 nH

5.2.2. The Frequency-Dependent S-Parameter Plots

The frequency-dependent S-parameters can be calculated by inverting the generalized **F**-matrix in Eq. (32) to demonstrate the spectral behavior of the ring hybrid. The transmission coefficients for the conventional and metamaterial ring hybrids, depicted in Fig. 12, show an equal power division at the design frequency between ports 2 and 3. The metamaterial hybrid suppresses the 2.7 GHz mode by approximately 17 dB. Excellent reflection and isolation characteristics are observed for both hybrids as given in Fig. 13.

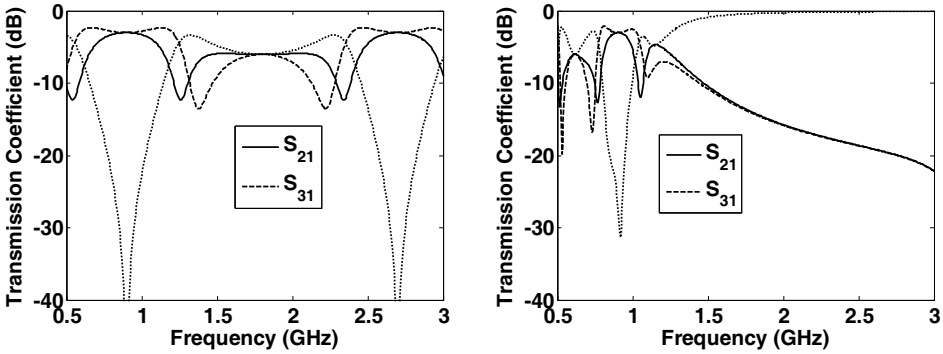

Figure 12. The Transmission coefficients observed at ports 2 and 3 of (a) a conventional ring hybrid and (b) a metamaterial ring hybrid.

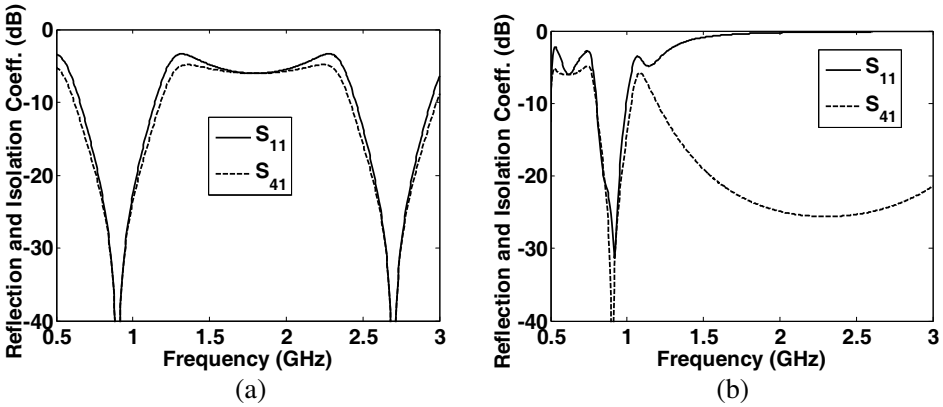

Figure 13. The reflection and isolation coefficients observed at ports 1 and 4 of (a) a conventional ring hybrid and (b) a metamaterial ring hybrid.

5.3. The Wilkinson Power Divider

The Wilkinson power divider is a passive 3-port microwave device which provides an equal power split at output with zero phase difference and a very good isolation [5, 6, 24]. Schematic diagrams of the conventional and metamaterial devices are shown in Fig. 14. The metamaterial power divider is obtained by replacing the $\lambda/2$ transmission line segments by four metamaterial unit-cells (Fig. 2(b))

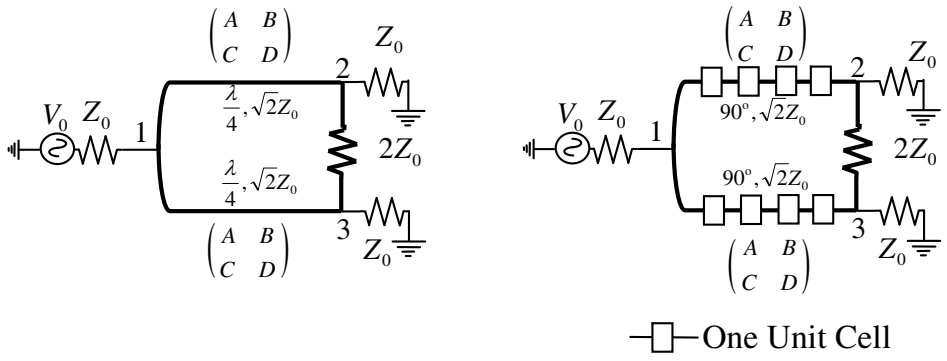

(a) Conventional Wilkinson Power Divider (b) Metamaterial Wilkinson Power Divider

Figure 14. The schematic diagram of (a) conventional Wilkinson power divider and (b) a metamaterial Wilkinson power divider.

whose parameters are given in Table 2. The application of the **F**-matrix generation rules results in:

$$\bar{F} = \begin{pmatrix} 2\dfrac{A}{B} + \dfrac{A_Z}{B_Z} & -\dfrac{1}{B} & -\dfrac{1}{B} \\ -\dfrac{1}{B} & \dfrac{A}{B} + \dfrac{3A_Z}{2B_Z} & -\dfrac{1}{2Z_0} \\ -\dfrac{1}{B} & -\dfrac{1}{2Z_0} & \dfrac{A}{B} + \dfrac{3A_Z}{2B_Z} \end{pmatrix} \tag{38}$$

At the design frequency, the **F**-matrix and its inverse for the conventional and the metamaterial device are given by:

$$\bar{F} = \frac{1}{Z_0}\begin{pmatrix} 1 & \pm\dfrac{j}{\sqrt{2}} & \pm\dfrac{j}{\sqrt{2}} \\ \pm\dfrac{j}{\sqrt{2}} & \dfrac{3}{2} & \mp\dfrac{1}{2} \\ \pm\dfrac{j}{\sqrt{2}} & \mp\dfrac{1}{2} & \dfrac{3}{2} \end{pmatrix}, \quad \bar{F}^{-1} = \frac{Z_0}{2}\begin{pmatrix} 1 & \mp\dfrac{j}{\sqrt{2}} & \mp\dfrac{j}{\sqrt{2}} \\ \mp\dfrac{j}{\sqrt{2}} & 1 & 0 \\ \mp\dfrac{j}{\sqrt{2}} & 0 & 1 \end{pmatrix} \tag{39}$$

where all the top-placed signs indicate the conventional power divider parameters. Assuming the input at nodes 1 and 2, respectively, the following two solutions of S-parameters are obtained:

$$\begin{bmatrix} V_1 \\ V_2 \\ V_3 \end{bmatrix} = \begin{bmatrix} S_{11}/2 - 1/2 \\ S_{21}/2 \\ S_{31}/2 \end{bmatrix} = \frac{Z_0}{2}\begin{pmatrix} 1 & \mp\dfrac{j}{\sqrt{2}} & \mp\dfrac{j}{\sqrt{2}} \\ \mp\dfrac{j}{\sqrt{2}} & 1 & 0 \\ \mp\dfrac{j}{\sqrt{2}} & 0 & 1 \end{pmatrix}\begin{pmatrix} \dfrac{1}{Z_0} \\ 0 \\ 0 \end{pmatrix} = \begin{bmatrix} \dfrac{1}{2} \\ \mp\dfrac{j}{2\sqrt{2}} \\ \mp\dfrac{j}{2\sqrt{2}} \end{bmatrix} \tag{40}$$

$$\begin{bmatrix} V_1 \\ V_2 \\ V_3 \end{bmatrix} = \begin{bmatrix} S_{12} \\ S_{22}/2 - 1/2 \\ S_{32}/2 \end{bmatrix} = \frac{Z_0}{2}\begin{pmatrix} 1 & \mp\dfrac{j}{\sqrt{2}} & \mp\dfrac{j}{\sqrt{2}} \\ \mp\dfrac{j}{\sqrt{2}} & 1 & 0 \\ \mp\dfrac{j}{\sqrt{2}} & 0 & 1 \end{pmatrix}\begin{pmatrix} 0 \\ 1/Z_0 \\ 0 \end{pmatrix} = \begin{bmatrix} \mp\dfrac{j}{2\sqrt{2}} \\ 1/2 \\ 0 \end{bmatrix} \tag{41}$$

The transmission S_{32} between ports 2 and 3 is zero which indicates that the two ports are fully isolated at the design frequency. Combining the results of Eqs. (40) and (41) and invoking reciprocity,

Table 3. Summary of node analysis results for various microwave devices.

Microwave Device	Circuit Diagram	$Z_0\bar{F}$-Matrix	$\bar{S}$-Matrix
Conventional Quadrature Hybrid	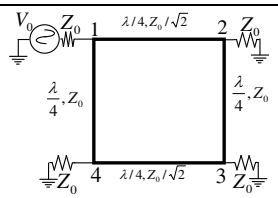	$\begin{pmatrix} 1 & +j\sqrt{2} & 0 & +j \\ +j\sqrt{2} & 1 & +j & 0 \\ 0 & +j & 1 & +j\sqrt{2} \\ +j & 0 & +j\sqrt{2} & 1 \end{pmatrix}$	$-\frac{1}{\sqrt{2}}\begin{pmatrix} 0 & +j & 1 & 0 \\ 1 & 0 & 0 & 1 \\ +j & 0 & 0 & +j \\ 0 & 1 & +j & 0 \end{pmatrix}$
Metamaterial Quadrature Hybrid	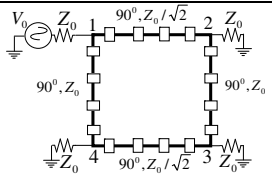	$\begin{pmatrix} 1 & -j\sqrt{2} & 0 & -j \\ -j\sqrt{2} & 1 & -j & 0 \\ 0 & -j & 1 & -j\sqrt{2} \\ -j & 0 & -j\sqrt{2} & 1 \end{pmatrix}$	$-\frac{1}{\sqrt{2}}\begin{pmatrix} 0 & -j & 1 & 0 \\ 1 & 0 & 0 & 1 \\ -j & 0 & 0 & -j \\ 0 & 1 & -j & 0 \end{pmatrix}$
Conventional 180° Hybrid (Rat-Race Coupler)	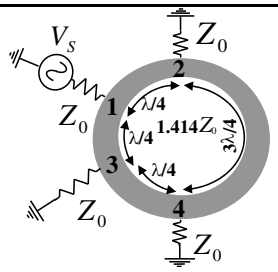	$\begin{pmatrix} 1 & +\frac{j}{\sqrt{2}} & +\frac{j}{\sqrt{2}} & 0 \\ +\frac{j}{\sqrt{2}} & 1 & 0 & -\frac{j}{\sqrt{2}} \\ +\frac{j}{\sqrt{2}} & 0 & 1 & +\frac{j}{\sqrt{2}} \\ 0 & -\frac{j}{\sqrt{2}} & +\frac{j}{\sqrt{2}} & 1 \end{pmatrix}$	$-\frac{j}{\sqrt{2}}\begin{pmatrix} 0 & 1 & 1 & 0 \\ 1 & 0 & 0 & -1 \\ 1 & 0 & 0 & 1 \\ 0 & -1 & 1 & 0 \end{pmatrix}$
Metamaterial 180° Hybrid (Rat-Race Coupler)	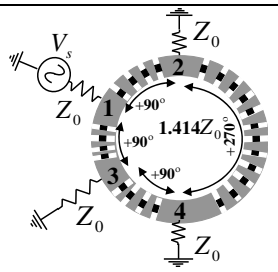	$\begin{pmatrix} 1 & -\frac{j}{\sqrt{2}} & -\frac{j}{\sqrt{2}} & 0 \\ -\frac{j}{\sqrt{2}} & 1 & 0 & +\frac{j}{\sqrt{2}} \\ -\frac{j}{\sqrt{2}} & 0 & 1 & -\frac{j}{\sqrt{2}} \\ 0 & +\frac{j}{\sqrt{2}} & -\frac{j}{\sqrt{2}} & 1 \end{pmatrix}$	$+\frac{j}{\sqrt{2}}\begin{pmatrix} 0 & 1 & 1 & 0 \\ 1 & 0 & 0 & -1 \\ 1 & 0 & 0 & 1 \\ 0 & -1 & 1 & 0 \end{pmatrix}$
Conventional Wilkinson Power Divider	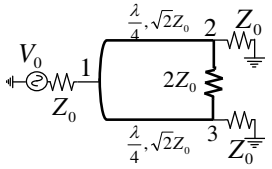	$\begin{pmatrix} 1 & +\frac{j}{\sqrt{2}} & +\frac{j}{\sqrt{2}} \\ +\frac{j}{\sqrt{2}} & \frac{3}{2} & -\frac{1}{2} \\ +\frac{j}{\sqrt{2}} & -\frac{1}{2} & \frac{3}{2} \end{pmatrix}$	$-\frac{1}{\sqrt{2}}\begin{pmatrix} 0 & j & j \\ j & 0 & 0 \\ j & 0 & 0 \end{pmatrix}$
Metamaterial Wilkinson Power Divider	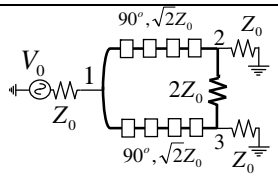	$\begin{pmatrix} 1 & -\frac{j}{\sqrt{2}} & -\frac{j}{\sqrt{2}} \\ -\frac{j}{\sqrt{2}} & \frac{3}{2} & +\frac{1}{2} \\ -\frac{j}{\sqrt{2}} & +\frac{1}{2} & \frac{3}{2} \end{pmatrix}$	$+\frac{1}{\sqrt{2}}\begin{pmatrix} 0 & j & j \\ j & 0 & 0 \\ j & 0 & 0 \end{pmatrix}$

the S-matrix of the power divider is obtained:

$$\bar{S} = \mp \frac{1}{\sqrt{2}} \begin{pmatrix} 0 & j & j \\ j & 0 & 0 \\ j & 0 & 0 \end{pmatrix} \tag{42}$$

The S-parameter spectra for the two power dividers, obtained by solving the simultaneous set of Equations (39)–(41), are shown in Fig. 15. An equal power division and excellent isolation and reflection properties are observed at the design frequency. The third harmonic mode at 2.7 GHz is well suppressed by about 10 dB in the metamaterial power divider.

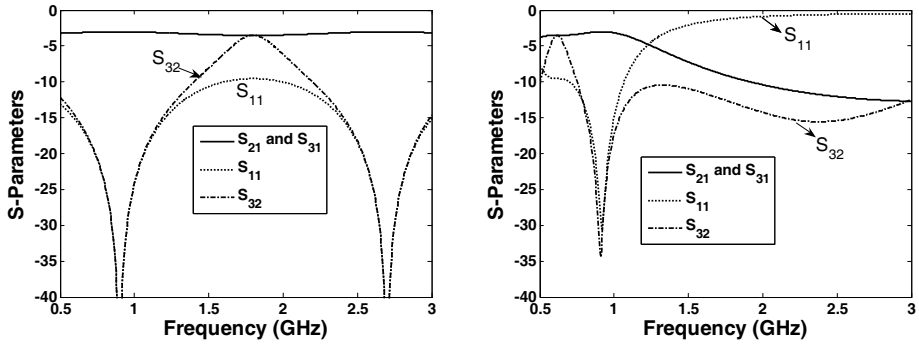

Figure 15. The S-parameters including transmission, reflection, and isolation coefficients for (a) a conventional Wilkinson power divider and (b) a metamaterial Wilkinson power divider.

5.4. Summary of the Microwave Device Node Analyses

Table 3 provides a summary of the node analyses of the three microwave devices that have been studied in the previous sub-sections. The **F**-matrix represents the coefficients of the node equations. The nth column of the **S**-matrix is obtained by assuming the source at the nth node and multiplying the $\mathbf{F}^{-1}$-matrix with the source array [Eq. (9)]. Note that the **F** and **S** matrices of the metamaterial device can be obtained from that of its conventional counterpart by substituting j with $-j$, indicating the backward wave propagation.

6. CONCLUSION

In this paper, we present a node analysis technique based on forward transmission matrix (FTM) which incorporates the electromagnetic traveling wave. Hence it can be used to solve electric circuits and networks at the microwave and higher frequency spectra in which the traditional node analysis does not work. In the proposed method, the node voltage equations are written by the modified Kirchhoff's circuit laws, and then the resulting **F**-matrix is solved by matrix inversion. The FTM method is used to compare wave propagation in some traditional microwave circuits and their metamaterial equivalents. The S-matrix for all configurations is determined by a systematic approach with methods rooted in circuit theory which are otherwise solved by theoretically challenging methods such as even-odd analysis methods in the contemporary textbooks. The proposed FTM method is a natural extension to the low-frequency traditional node analysis. Consequently, it offers a smooth transition for an electrical engineering student coming from low-frequency electronics to microwave circuits.

ACKNOWLEDGMENT

This research is supported by the Deanship of Scientific Research, Taibah University under the Project number 4611 for the year 2015–2016.

APPENDIX A. DESIGN OF THE METAMATERIAL UNIT CELL

The design approach is outlined in [20] and [24]. Here it is given for completeness. Considering the unit cell of Fig. 2, the Bloch phase shift 'kd' (phase shift per unit cell) can be written in the form of the following dispersion equation [21]:

$$\cosh kd = \cos\beta d\left[1+\frac{Y_{sh}Z_s}{4}\right]+\frac{j}{2}\sin\beta d\left[Z_sY_o+Y_{sh}Z_U\right]+\frac{Y_{sh}Z_s}{4} \tag{A1}$$

where Z_U and β are the intrinsic characteristic impedance and phase constant of the underlying host transmission line. Z_s and Y_{sh} are the series impedance and shunt impedance loading elements in the unit cell. For small phase shifts, the Bloch phase (θ_B) and Bloch impedance (Z_B) can be approximated as [15, 21]:

$$\theta_B^2 = L'C'\frac{(\omega_1^2-\omega^2)(\omega_2^2-\omega^2)}{\omega^2} \tag{A2}$$

$$Z_B^2 = \frac{L'}{C'}\frac{(\omega_1^2-\omega^2)}{(\omega_2^2-\omega^2)} \tag{A3}$$

Here $L' = L_0d$. $C' = C_0d$ for the traditional metamaterial (Fig. 2(a)) and $C' = C_{0d} + C_{sh}$ for the capacitor-loaded metamaterial-TL (Fig. 2(b)). L_0 and C_0 are the distributed inductance and capacitance of the host transmission line and are given below in terms of the phase velocity (u) of the medium:

$$L_o = Z_U/u \quad \text{and} \quad C_o = 1/Z_Uu \tag{A4}$$

The radian frequencies ω_1 and ω_2 identify the cutoff frequencies of the first and second fundamental harmonics and will be explained later in this section. These cutoff frequencies are expressed in terms of the already defined inductances and capacitances as follows:

$$\omega_2 = \frac{1}{L_{sh}C'} \quad \text{and} \quad \omega_1 = \frac{1}{L'C_s} \tag{A5}$$

To obtain the unit-cell elements (C_s, L_{sh}, C_{sh}, and d), we have to identify the design frequency ω. The distributed inductance per unit-cell length is then given by multiplying Eqs. (A2) and (A3):

$$L' = \frac{\theta_BZ_B\omega}{\omega_1^2-\omega^2} \tag{A6}$$

Dividing Eq. (A2) by Eq. (A3) and rearranging results in,

$$C' = \frac{\theta_B\omega}{Z_B(\omega_2^2-\omega^2)} \tag{A7}$$

C_s and L_{sh} can then be evaluated from Eq. (A5). For the conventional metamaterial design, the characteristic impedance Z_0 and periodicity d can be found by applying the following formulas:

$$d = \frac{L'}{L_0} \quad \text{and} \quad Z_0 = \sqrt{\frac{L'}{C'}} \tag{A8}$$

Note that before finding the periodicity d, the distributed inductance and capacitance are calculated from relations (A4). On the other hand, for the capacitor loaded metamaterial-TL, the distributed capacitance can be found by first assuming an appropriate value for $C_{sh} < C'$ and then applying $C_0d_{=}C' - C_{sh}$. Finally, the characteristic impedance and the periodicity of the host line can be found by:

$$Z_0 = \sqrt{\frac{L'}{C_0d}} \quad \text{and} \quad d = \frac{C_0d}{C_0} \tag{A9}$$

REFERENCES

1. Alexander, C. K. and M. N. Sadiku, *Fundamentals of Electrical Engineering*, 5th edition, 82, Mc. Graw Hill, New York, NY, 2013.
2. Chen, W.-K., *The Electrical Engineering Handbook*, 8, El Sevier Academic Press, Burlingtron, MA, 2004.
3. Khalil, A. I. and M. B. Steer, "Circuit theory for spatially distributed microwave circuits," *IEEE Trans Micro. Theory Tech.*, Vol. 46, 1500–1502, 1998.
4. Smith, C., "Frequency domain analysis of RF and microwave circuits using SPICE," *IEEE Trans Micro. Theory Tech.*, Vol. 42, 1904–1909, 1994.
5. Pozar, D., *Microwave Engineering*, 3rd edition, 49–55, 183–187, 257–260, 318–358, John Wiley & Sons, 2005.
6. Collin, R. E., *Foundations of Microwave Engineering*, 2nd edition, 85–96, 413–449, IEEE Press, 2001.
7. Shelby, R. A., D. R. Smith, S. Shultz, and S. C. Nemat-Nasser, "Microwave transmission through a two-dimensional, isotropic, left-handed metamaterial," *App. Phys. Lett.*, Vol. 78, 489–491, 2001.
8. Smith, D. R., W. Padilla,, D. Vier, S. Nemat-Nasser, S. Schultz, "Composite medium with simultaneously negative permeability and permittivity," *Phys. Rev. Lett.*, Vol. 84, 4184–4187, 2000.
9. Caloz, C. and Itoh T., *Electromagnetic Metamaterials: Transmission Line Theory and Microwave Applications*, 1st edition, John Wiley & Sons, 2006.
10. Eleftheriades, G. V. and K. G. Balmain, *Negative Refraction Metamaterials: Fundamental Principles and Applications*, 1st edition, John Wiley & Sons, 2005.
11. Nader, E. and R. W. Ziolkowski, *Metamaterials: Physics and Engineering Explorations*, 3–30, 37, 143–150, 215–234, 240–256, Wiley & Sons, 2006.
12. Zouhdi, S., A. Sihvola, and A. P. Vinogradov, *Metamaterials and Plasmonics: Fundamentals, Modelling, Applications*, Springer-Verlag, New York, December 2008.
13. Xu, H., G. Wang, and Q. Peng, *Novel Resonant-Type Composite Right/Left Handed Transmission Line Based on Cascaded Complementary Single Split Ring Resonator In Electrical Engineering and Control*, Vol. 2, 98–107, Springer-Verlag, Berlin, Heidelberg, 2011.
14. Bala, B. D., M. K. Rahim, and N. A. Murad, Composite right/left-handed dual-band metamaterial antenna with improved gain and efficiency," *Microw. Opt. Tech. Lett.*, Vol. 56, 1575–1579, 2014.
15. Siddiqui, O., A. Mohra, and G. Eleftheriades, "Quad-band power divider based on left-handed transmission lines," *Elect. Lett.*, Vol. 46, 1441–1442, 2010.
16. Eleftheriades, G., "EM transmission-line metamaterials," *Materials Today*, Vol. 12, 30–41, 2009.
17. Antoniades, M. A. and G. V. Eleftheriades, "Compact, linear, lead/lag metamaterial phase shifters for broadband applications," *IEEE Antenn. Wireless Propag. Lett.*, Vol. 2, 103–106, 2001.
18. Hu, J., J. Xiong, T. Ling, and Y. Zou, "Design of a novel Wilkinson power splitter based on the left-handed transmission line," *Microw. Opt. Tech. Lett.*, Vol. 49, 2975–2977, 2007.
19. Qureshi, F., M. A. Antoniades, and G. V. Eleftheriades, "A compact and low-profile metamaterial ring antenna with vertical polarization," *IEEE Antenn. Wireless Propag. Lett.*, Vol. 4, 333–336, 2005.
20. Siddiqui, O. and A. Mohra, "A harmonic-suppressed microstrip antenna using a metamaterial-inspired compact shunt-capacitor loaded feedline, *Progress In Electromagnetics Research C*, Vol. 45, 151–162, 2013.
21. Siddiqui, O., M. Mojahedi, and G. V. Eleftheriades, "Periodically loaded transmission line with effective negative refractive index and negative group velocity," *IEEE Trans. on Antenn. and Propag.*, Vol. 51, 2619–2625, 2003.
22. Siddiqui, O. and G. V. Eleftheriades, "Study of resonance-cone propagation in truncated hyperbolic metamaterial grids using transmission-line matrix simulations," *Journal of Franklin Institute*, Vol. 348, 1285–1297, 2011.

23. Siddiqui, O., "Numerical investigation of phase and group propagation of time-domain signals in a novel band-reject metamaterial ring hybrid," *Journal of Computer and Communications*, Vol. 3, 10–17, doi: 10.4236/jcc.2015.36002, 2015.
24. Siddiqui, O., "Dispersion analysis of capacitive loaded negative-refractive-index transmission lines and associated applications," *8th International Symposium on Antennas, Propagation and EM Theory, (ISAPE 2008)*, 698–701, Kunming, China, 2008.